11-12-2015

Effect of genetic background on the dystrophic phenotype in mdx mice.

William D Coley

Laurent Bogdanik

Maria Candida Vila

Qing Yu

Terence A Partridge
George Washington University

See next page for additional authors

Recommended Citation

Coley WD, Bogdanik L, Vila MC, Yu Q, Van Der Meulen JH, Rayavarapu S, Novak JS, Nearing M, Quinn JL, Saunders A, Dolan C, Andrews W, Lammert C, Austin A, Partridge TA, Cox GA, Lutz C, Nagaraju K. (2015). Effect of genetic background on the dystrophic phenotype in mdx mice. Human Molecular Genetics. pii: ddv460. [Epub ahead of print]

Authors
William D Coley, Laurent Bogdanik, Maria Candida Vila, Qing Yu, Terence A Partridge, Kanneboyina Nagaraju, and +12 additional authors

Human Molecular Genetics, 2016, Vol. 25, No. 1 130–145

doi: 10.1093/hmg/ddv460
Advance Access Publication Date: 12 November 2015
Original Article

ORIGINAL ARTICLE

Effect of genetic background on the dystrophic phenotype in *mdx* mice

William D. Coley[1,†], Laurent Bogdanik[2,†], Maria Candida Vila[1,3], Qing Yu[1], Jack H. Van Der Meulen[1], Sree Rayavarapu[1], James S. Novak[1], Marie Nearing[1], James L. Quinn[1], Allison Saunders[2], Connor Dolan[2], Whitney Andrews[2], Catherine Lammert[2], Andrew Austin[2], Terence A. Partridge[1], Gregory A. Cox[2], Cathleen Lutz[2,*] and Kanneboyina Nagaraju[1,3,*]

[1]Research Center for Genetic Medicine, Children's National Health System, Washington, DC, USA, [2]The Jackson Laboratory, Bar Harbor, ME, USA and [3]Department of Integrative Systems Biology, George Washington University School of Medicine, Washington, DC, USA

*To whom correspondence should be addressed at: Research Center for Genetic Medicine, Children's National Health System, 111 Michigan Avenue, N.W. Washington, DC 20010, USA, Tel: +1 2024766220; Fax: +1 2024766014; Email: knagaraju@childrensnational.org (K.N.); The Jackson Laboratory, 610, Main Street Bar Harbor, ME 04609, USA. Tel: +1 2072886341; Fax: +1 2072886149; Email: cat.lutz@jax.org (C.L.)

Abstract

Genetic background significantly affects phenotype in multiple mouse models of human diseases, including muscular dystrophy. This phenotypic variability is partly attributed to genetic modifiers that regulate the disease process. Studies have demonstrated that introduction of the γ-sarcoglycan-null allele onto the DBA/2J background confers a more severe muscular dystrophy phenotype than the original strain, demonstrating the presence of genetic modifier loci in the DBA/2J background. To characterize the phenotype of dystrophin deficiency on the DBA/2J background, we created and phenotyped DBA/2J-congenic Dmdmdx mice (D2-mdx) and compared them with the original, C57BL/10ScSn-Dmdmdx (B10-mdx) model. These strains were compared with their respective control strains at multiple time points between 6 and 52 weeks of age. Skeletal and cardiac muscle function, inflammation, regeneration, histology and biochemistry were characterized. We found that D2-mdx mice showed significantly reduced skeletal muscle function as early as 7 weeks and reduced cardiac function by 28 weeks, suggesting that the disease phenotype is more severe than in B10-mdx mice. In addition, D2-mdx mice showed fewer central myonuclei and increased calcifications in the skeletal muscle, heart and diaphragm at 7 weeks, suggesting that their pathology is different from the B10-mdx mice. The new D2-mdx model with an earlier onset and more pronounced dystrophy phenotype may be useful for evaluating therapies that target cardiac and skeletal muscle function in dystrophin-deficient mice. Our data align the D2-mdx with Duchenne muscular dystrophy patients with the LTBP4 genetic modifier, making it one of the few instances of cross-species genetic modifiers of monogenic traits.

Introduction

Genetic backgrounds affect disease phenotype in both mice and humans, for example in models for amyotrophic lateral sclerosis (ALS) or muscular dystrophy and patients with mutations causing ALS (1–4). A stop codon mutation within exon 23 of the mouse dystrophin gene (Dmd) on the X chromosome results in

[†]W.D.C. and L.B. contributed equally to the study.

Received: July 9, 2015. **Revised and Accepted:** November 5, 2015

the absence of dystrophin (5,6). The skeletal muscles in these mice on a C57BL/10 (B10) background (C57BL/10-*mdx* mice) undergo cycles of degeneration and regeneration, along with infiltration of immune cells and elevated levels of serum creatine kinase (CK). As compared with B10 wild-type control mice, both male and female *mdx* mice have reduced life spans (7). These mice do not typically show significant fatty replacement or fibrosis in the skeletal muscle. However, unlike the skeletal muscle, the diaphragm in dystrophin-deficient mice undergoes extensive progressive degeneration, mineralization and regeneration, followed by fibrosis and a loss of myofibers (8). Despite the milder phenotype in skeletal muscle, these mice are routinely used in preclinical evaluations because they are genetic and biochemical homologs of human Duchenne muscular dystrophy (DMD). In fact, the B10-*mdx* mouse is the most widely used mouse model for DMD.

Genetic mapping studies performed in Dr. Elizabeth McNally's group have shown that the introduction of the mouse sarcoglycan gamma (*Sgcg*)-null allele onto the DBA/2J genetic background confers a more severe muscular dystrophy phenotype than that in the 129T2/SvEmsJ strain, demonstrating that genetic modifier loci in the DBA/2J background affect the disease phenotype of *Sgcg*-null mice. Furthermore, this group identified one of the genetic loci responsible for the difference in the severity of the phenotypes of the Sgcg-null mutation in 129T2/SvEmsJ and DBA/2. They found that a polymorphism in the coding region of the latent TGF-β-binding protein 4 gene (Ltbp4) results in a 12-amino acid deletion in LTBP4 in the DBA/2 mice. This deletion is associated with increased proteolysis, SMAD signaling and fibrosis, and the proposed mechanism is that Ltbp4, which down-regulates TGF-β signaling in its full-length form, is less active in DBA/2 mice, thus allowing a stronger inflammation response to the loss-of-function of Sgcg; this, in turn, worsens the associated muscle pathology and modifies the outcome of the muscular dystrophy in this model (9). Beside a reduced TGF-β signaling, DBA/2 mice also present with a lower self-renewal efficiency of the satellite cells than that of C57BL/6 mice. Based on this finding, Fukada *et al.* generated a DBA/2-*mdx* strain by crossing DBA/2 and C57BL/10-*mdx*. They found that the hind limb muscles of DBA/2-*mdx* mice exhibited increased weakness, lower muscle weight, fewer myofibers and increased fat and fibrosis when compared with B10-*mdx* mice, suggesting that the satellite cells' self-renewal ability may be one of reasons for the differences in pathology between these mouse strains (10).

The human LTBP4 locus has been similarly shown to be a genetic modifier of disease severity in DMD patients. A four-locus haplotype in the LTBP4 gene was shown to be associated with age at loss of ambulation (11). Patients with the homozygous IAAM amino acid haplotype showed approximately a 2-year later loss of ambulation compared with other genotypes. This finding was validated in two additional DMD cohorts (12,13). These findings suggest that studies of the mdx mutation modified by LTBP4 polymorphisms (DBA background) in mice are highly relevant to the human DMD disease, and likely predictive of human pathophysiology.

To further investigate the effect of genetic background on the dystrophic phenotype, we have re-created a DBA/2J-congenic DMD *mdx* (D2-*mdx* strain) mouse model with a better defined genetic make-up (see Materials and Methods). Contrary to the approach previously used to make the first congenic mice, we used an SNP-panel-assisted breeding strategy that allowed us to exclude most of the original C57BL/10J genome from the new D2.B10 mdx congenic (see Materials and Methods). We have systematically assessed the functional, histological, biochemical and molecular phenotype of these mice at 7, 28 and 52 weeks of age and compared them with the standard B10-*mdx* and the two respective background control strains (DBA/2 and C57BL/10), thereby extending the age range studied by Fukada *et al.* (10). Some of the parameters were assessed and reproduced in two different laboratories [the Children's National Medical Center (CNMC) and The Jackson Laboratory] in independent cohorts of mice. We also analyzed muscular dystrophy features that were not documented in the first report, namely the cardiomyopathy, mRNA expression profiles of the skeletal muscles and inflammation. We found that D2-mdx mice showed significantly reduced cardiac and skeletal muscle function and increased inflammation, suggesting that genetic background significantly affects the disease phenotype of dystrophic mice.

Results

Body weight

The body weights for mice were measured at 7, 28 and 52 weeks of age (Supplementary Material, Table S1). We compared body weights recorded at the 28-week time point at both the CNMC (Fig. 1A) and The Jackson Laboratory (Fig. 1B). We found that B10-*mdx* mice were generally bigger than the B10 controls, whereas the D2-*mdx* mice were significantly smaller than the DBA/2 control mice. The two wild-type strains (B10 and D2) were not significantly different from each other at this age, whereas D2-*mdx* mice were significantly smaller than the B10-*mdx* mice. The differences in the body weights between the *mdx* and wild-type strains were consistent between the two laboratories (Fig. 1A and B).

Tissue weights

We examined the weights of the gastrocnemius, tibialis anterior (TA) and quadriceps muscles and the heart and spleen tissues in all strains (Supplementary Material, Table S1). We found that the muscle weights of the two control strains were the most similar. For all three muscles, the B10-*mdx* mice showed an increase in muscle mass. In contrast, D2-*mdx* mice showed a loss of muscle mass in all three muscles at all time points when compared with the D2 mice. The muscle/body weight ratios for many muscles were lower in the D2-*mdx* than in D2 mice from the 28th week on, suggesting a muscle atrophy, whereas the muscle/body weight ratios in B10-*mdx* were higher than in B10 mice, reflecting

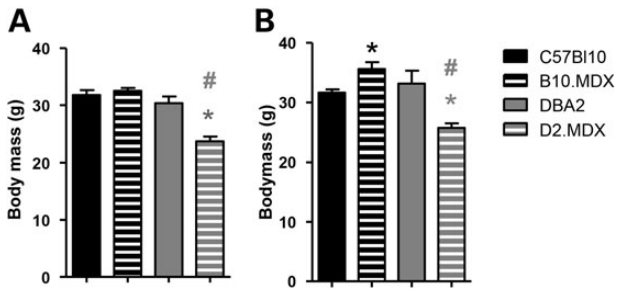

Figure 1. Loss of body mass in the D2-*mdx* strain was observed independently. Body mass was recorded for all four strains independently at both CNMC (**A**) and The Jackson Laboratory (**B**). Results for body weights taken at 28 weeks are shown. Significant differences within the same genetic background are marked with the asterisk symbol. Significant differences between the two *mdx* strains are marked with the hash symbol. B10-*mdx* mice were heavier than their B10 wild-type controls as expected. In contrast, the D2-*mdx* strain was consistently smaller than D2 control. $n = 6$ mice per group, average ± SEM).

the well-documented muscle hypertrophy of this model. We also found that the mass of the heart differed significantly between the two control strains. The mass of the heart did not differ between strains at 7 weeks of age, but with age, the D2 hearts became significantly larger than the B10 hearts. This increase in cardiac mass was mirrored in the D2-*mdx* mice, whose hearts were similar in size to those of the D2 strain. However, the B10-*mdx* mice were also observed to have enlarged hearts, relative to the BL10 controls, although this enlargement was significant only at the last time point.

Fiber diameter measurement

To determine the effect of genetic background on muscle fiber diameter, we evaluated the average diameter of the muscle fibers in the TA muscle. Cross sections of the fixed TA muscle were stained for reticulin in order to clearly mark muscle fiber perimeters. Representative images of reticulin staining are shown in Figure 2A. We found that the average fiber diameters were shifted in opposite directions by the *mdx* mutation, depending on the background strain. B10-*mdx* mice were found to have fewer normal-sized fibers (375–1500 m^2) and a greater proportion of hypertrophic fibers (>1500 m^2) (Fig. 2B). This observation is consistent with prior findings of hypertrophy in this strain (14). In contrast, the D2-*mdx* mice were found to have relatively few hypertrophic fibers alongside a large number of small fibers. Specifically, the average fiber diameter was reduced to 375 m^2, from the average of 750 m^2 seen in control DBA/2 mice. These results are consistent with our findings regarding changes in muscle mass and muscle/body weight ratios between the two strains.

Creatine kinase enzyme activity

Serum CK enzyme activity was determined at 28 weeks of age by both the CNMC (Fig. 3A) and The Jackson Laboratory (Fig. 3B). The two control strains (B10 and D2) were found to have minimal amounts of CK activity. Both *mdx*-mutant strains were observed to have significantly elevated levels of serum CK activity when

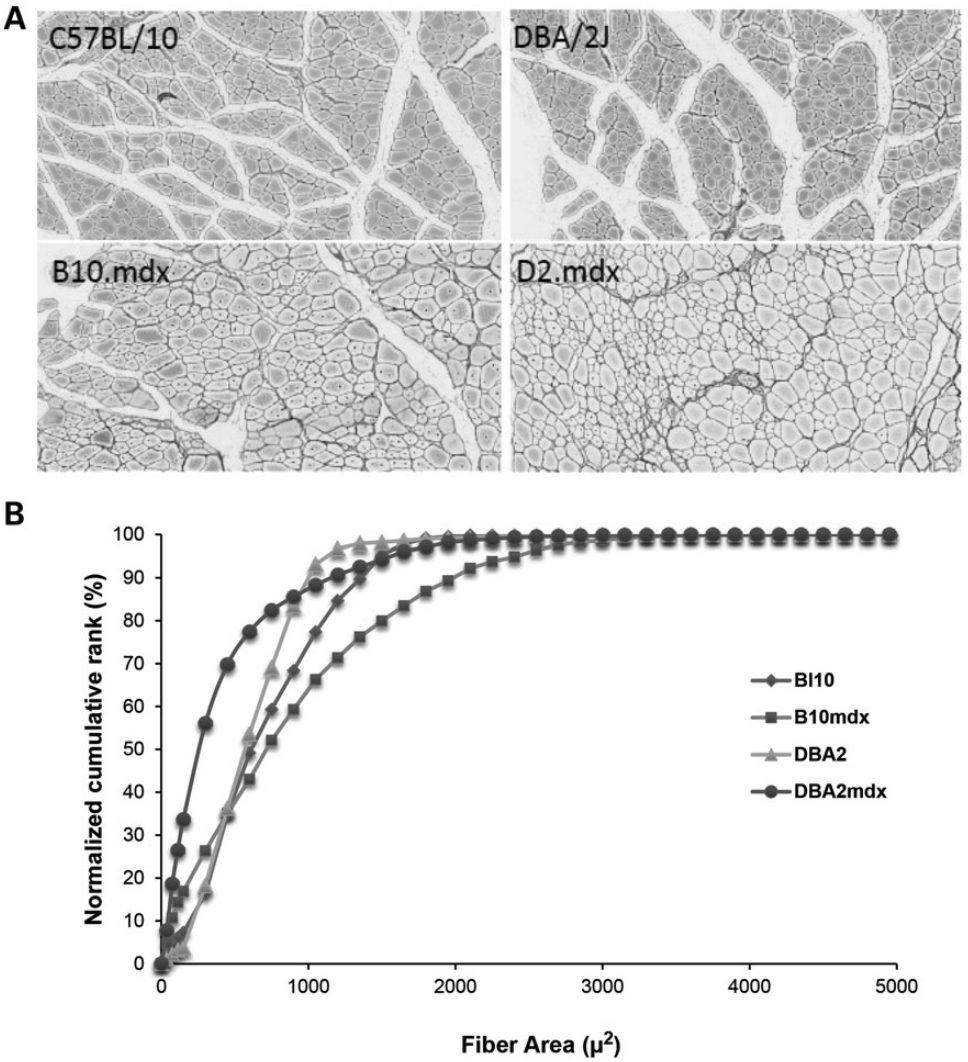

Figure 2. D2-*mdx* mice do not exhibit the hypertrophy that is seen in B10-*mdx* mice. The TA from each mouse was dissected at 12 weeks and preserved in 4% formalin prior to staining for reticulin (**A**). Fiber area was then measured for each strain as shown in (**B**). The plot shows the fiber areas that were ranked by size, averaged and expressed as a percentage of the total fiber sample for each strain: B10, B10-*mdx*, D2, D2-*mdx*. Statistical analysis was performed by the Kolmogorov–Smirnov (K–S) two-sample test; B10 versus D2, $P = 0.034$; B10 versus B10-mdx, $P = 0.018$; D2 versus D2-mdx, $P = 0.341$; B10-mdx versus D2-mdx, $P = 0.039$. $n = 4$ (B10-*mdx* and D2-*mdx*), 6 (B10) and 8 (D2) mice per group.

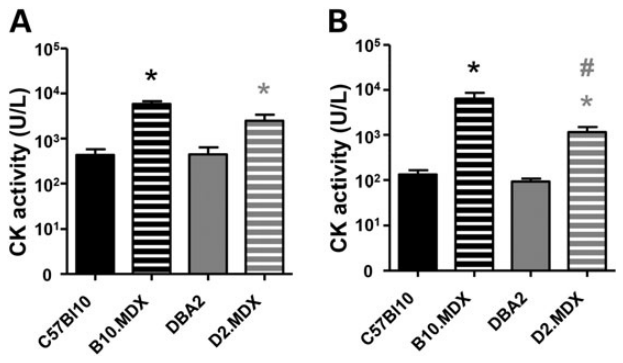

Figure 3. Both *mdx* strains show similar serum CK profiles. Levels of CK enzyme activity in the serum from all four strains were measured at 28 weeks at CNMC (**A**) and at 24 weeks at The Jackson Laboratory (**B**). The results were consistent between the two labs. Serum CK levels for D2-*mdx* mice were significantly higher than normal baseline levels but on average were lower than the levels seen in B10-*mdx* mice. $n = 8$ (B10.mdx), 11 (D2.mdx) and 12 (B10 and D2 controls) mice per group, average ± SEM.

compared with age-matched controls. D2-*mdx* mice showed relatively lower serum CK levels than did the B10-*mdx* mice at 24 weeks of age. The serum CK data were consistent between the two laboratories.

Evans blue dye uptake

Damage to muscle fibers can also be measured by quantifying the uptake of Evans blue dye (EBD) by the muscle tissue. Incorporated EBD can either be visualized via fluoroscopy in fixed tissues (Fig. 4A–D) or quantified in muscle lysates via spectroscopy (Fig. 4E). The quantification of EBD retained within these tissues confirmed that the two *mdx* strains had significant uptake when compared with their respective controls. However, the D2-*mdx* mice were found to have a significantly higher uptake of EBD than did the B10-*mdx* mice.

Grip strength

The grip-strength measure (GSM) for all four mouse strains was performed at both the CNMC and the Jackson Laboratory. At CNMC, GSM was measured at 28 and 52 weeks of age in the forelimbs and hindlimbs, and at The Jackson laboratory in the forelimbs at 6, 12 and 24 weeks of age (Supplementary Material, Fig. S1). Because of the differences in the body weights of the different strains, the forelimb and hindlimb maximal force (kgf) data were normalized to the body weight of the animal and are presented as normalized grip force (kgf/kg). There was an overall decline in grip strength in all strains by 52 weeks of age (Supplementary Material, Fig. S1). *mdx* mice on both backgrounds showed significantly lower normalized grip strength than did their respective control mouse strains in both laboratories at the 24- or 28-week time points (Fig. 5A and B). The normalized GSM data for the hindlimbs collected at the CNMC were consistent with the forelimb data collected at both laboratories.

In vitro extensor digitorum longus force contraction

The weights of the extensor digitorum longus (EDL) muscles showed that the D2 mice had significantly smaller EDL muscles than did the BL10 mice at 7 weeks of age, and these differences were reduced at the 28-week and 52-week time points. B10-*mdx* mice showed significantly more muscle mass than did control BL10 mice at 28 and 52 weeks of age, whereas D2-*mdx* mice showed a lower EDL mass than did the control D2 mice at 28 and 52 weeks of age (Fig. 6A).

We then evaluated the maximal force and specific force production of the EDL muscles but did not detect any significant differences in either the maximal or specific force between the two wild-type control strains at any time point. The maximal force shown by the EDL muscles of the BL10-*mdx* mice was similar to that of the BL10 controls at all time points (Fig. 6B). In contrast, the specific force significantly decreased at all time points in the BL10-*mdx* mice when compared with the BL10 controls (Fig. 6C). Unlike the BL10-*mdx* mice, the D2-*mdx* mice showed a significant reduction in both maximal and specific force at all three time points tested (Fig. 6B and C).

Echocardiography and cardiac function

The assessment of heart function was carried out using echocardiography on live, sedated mice. We found that the ejection fraction (EF) and shortening fractions (SF) were significantly higher at 7 weeks of age in the wild-type D2 mice than in the wild-type BL10 mice; heart weights were also significantly different between the two genotypes. However, cardiac output normalized to heart rate did not change when comparing wild-type D2 and BL10 mice, indicating that the increase in heart mass is not pathologically related to heart failure, because EF is maintained or increased in wild-type D2 mice (Supplementary Material, Table S1). Additionally, these differences were lost at 28 and 52 weeks of age. The D2-*mdx* mice showed a significantly lower EF and SF than did the control D2 strain, whereas the EF and SF values for the BL10-*mdx* and BL10 mice were similar at 28 weeks of age (Fig. 7 A and B). By 52 weeks of age, both strains showed significant deficits in EF and SF when compared with their respective wild-type strains. We also found a significant drop in stroke volume (Supplementary Material, Fig. S2A), and cardiac output (Supplementary Material, Fig. S2B) in both strains when compared with their wild-type controls.

Histological (H&E) evaluation of muscle tissues

We examined the diaphragm, quadriceps and heart muscles for muscle damage at 7, 28 and 52 weeks of age. Representative images for the diaphragm (Fig. 8A), heart (Fig. 8B) and quadriceps (Supplementary Material, Fig. S3) are shown for all four strains at all three time points. The histologic appearance of all three tissues was normal for the control BL10 and D2 strains at all time points. At 7 weeks, both *mdx* strains showed lesions exhibiting muscle degeneration, regeneration and mononuclear infiltrating cells within the quadriceps and diaphragm. In addition, the D2-*mdx* mice, but not the B10-*mdx* mice, showed significant calcification in all tissues. We also observed that the D2-*mdx* mice showed signs of inflammation within the cardiac tissue at 7 weeks of age, whereas the B10-*mdx* mice showed normal cardiac histology at that age.

To quantify the calcified deposits, we performed microCT scanning (Supplementary Material, Fig. S4A–C) and found that calcified deposits were distributed throughout the muscle tissue in the quadriceps, diaphragm and in the epicardium of the heart tissue. Overall, a significant increase in tissue density as early as at 7 weeks of age was seen only in the D2-*mdx* mice (Supplementary Material, Fig. S4D–F).

Optical imaging to monitor muscle inflammation

We have previously demonstrated that optical imaging of Cathepsin B (CTSB) activity in live mice using cathepsin caged

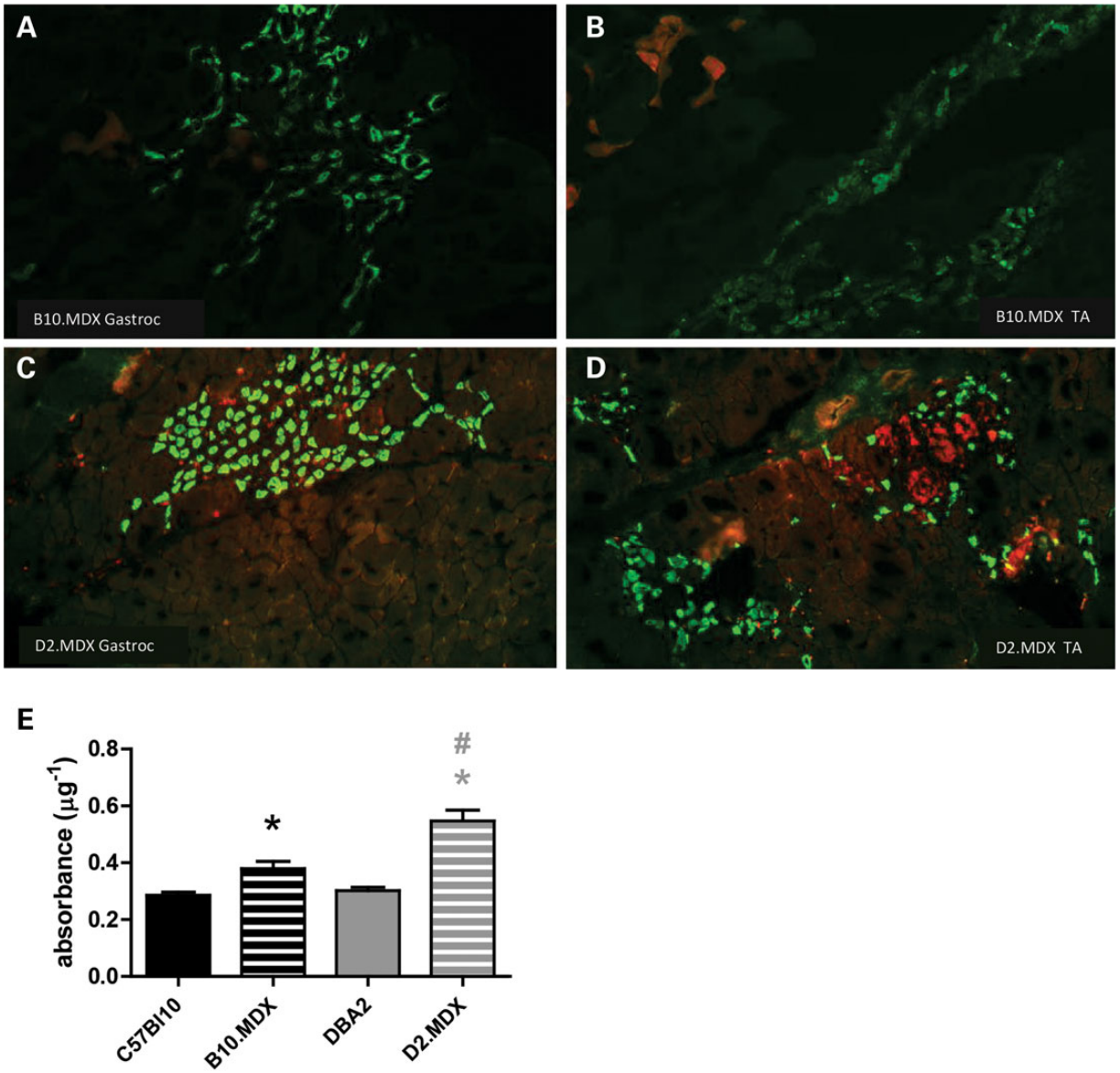

Figure 4. D2-*mdx* show increased levels of EBD uptake compared with B10-*mdx*. In order to quantify muscle fiber damage, the gastrocnemius and TA muscle were dissected from all four strains of mice at 8 weeks of age. All mice were injected with EBD 24 h prior to being sacrificed. Representative fluorescent cross sections from B10-*mdx* (**A, B**) and D2-*mdx* (**C, D**) muscles show retained EBD in red and positive myh3 staining in green. EBD absorbance from gastrocnemius lysates was quantified by spectroscopy and normalized to total protein concentration in grams. (**E**). $n = 8$ (B10.mdx), 9 (D2.mdx) and 12 (B10 and D2 controls) mice per group, average ± SEM.

near-infrared imaging is an ideal method to sensitively monitor inflammation and regeneration in dystrophic skeletal muscle (15). We evaluated cathepsin activity in all mouse strains at 7 and 52 weeks of age (Supplementary Material, Fig. S5) and found that cathepsin activity in the forelimb was similar between wild-type strains at both ages whereas hind limb cathepsin activity was higher in D2 mice at 7 weeks and decreased significantly at 52 weeks in comparison with BL10 mice. Both BL10.*mdx* and D2-*mdx* mice show highly significant elevation of cathepsin activity in both fore and hindlimbs at 7 weeks in comparison with wild-type control strains. D2-*mdx* but not BL10-*mdx* mice show significantly increased cathepsin activity at 52 weeks of age in comparison with their respective controls. The differences in cathepsin activity between the strains are less marked at 52 weeks of age (Fig. 9A and B).

QRT–PCR of inflammatory genes

To determine whether the components of the inflammatory process differed between the B10-*mdx* and D2-*mdx* mice, we analyzed the relative gene expression of 14 different inflammation-related transcripts in all four strains of mice. This QRT–PCR procedure was performed at CNMC using mRNA isolated from the TA muscle taken at the 7-week and 52-week time points. Similar QRT–PCR analyses were carried out at the Jackson Laboratory at the 12-week time point. In general, the results from both labs confirmed that there were significant differences between the two *mdx* strains. Figure 10 shows the change in relative expression over time for a select few of the assayed genes. A complete table of the QRT–PCR results from both laboratories is provided in Supplementary Material, Table S2. Pro-inflammatory cytokines such as TNF-alpha were consistently elevated at both

time points in the *mdx* strains when compared with their wild-type controls, whereas other pro-inflammatory cytokines such as IL-6 and IL-1-beta were increased at 52 weeks of age in both *mdx* strains when compared with their controls (Fig. 10). These two cytokines were significantly higher in the D2-*mdx* mice than in the B10-*mdx* mice. Some markers of macrophage migration (CCL2 and EMR1) were highly upregulated in both strains early in the disease and showed a significant decrease at a latter age. Type 1 IFNb was expressed to a greater extent in the control strains than in the *mdx* mouse strains.

Central nuclei and BrdU labeling

Central nucleated fibers are markers of muscle regeneration. Using H&E-stained sections, we quantified the percentage of centrally nucleated fibers in cross sections of B10-*mdx* and D2-*mdx* skeletal muscle (Fig. 11A and B). Both *mdx* strains showed significantly higher numbers of centrally nucleated fibers than in their respective wild-type strains, but the D2-*mdx* mice showed significantly fewer centrally nucleated fibers than did the B10-*mdx* mice (Fig. 11E).

To evaluate whether the turnover of myonuclei differs between the two *mdx* mouse strains, we added bromodeoxyuridine (BrdU) in their drinking water. BrdU is a nucleotide analog that is incorporated into newly synthesized DNA and can later be visualized by immunohistochemical staining. Representative images of BrdU-labeled muscles from B10-*mdx* and D2-*mdx* TA muscles are shown in Figure 11C and D. A comparison between the two *mdx* strains revealed foci of regeneration containing similar total numbers of BrdU-positive myonuclei within muscle fibers of the TA (Fig. 11F), but in the D2-*mdx* mice, these were predominantly located in a juxtasarcolemmal position whereas in the B10-*mdx* muscles they were predominantly centrally located (Fig. 11G).

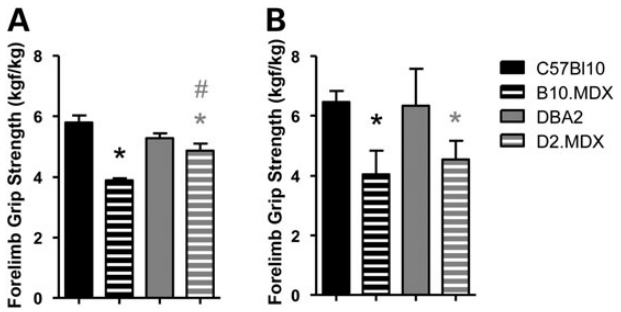

Figure 5. Loss of grip strength in the D2-*mdx* strain was observed independently. Forelimb grip strength was recorded for all four strains independently at both CNMC (**A**) and The Jackson Laboratory (**B**). Results for grip strength taken at 28 weeks are shown. All grip-strength measurements are normalized to the individual animal's body weight. Both *mdx* strains were significantly weaker than their wild-type controls. The same trends in forelimb grip strength were also reproducible between labs.

Myosin heavy chain expression

Muscle fibers express various homologs of the myosin heavy chain protein at various stages of development or repair. Embryonic and neonatal myosin genes (*Myh3* and *Myh8*, respectively) are markers for muscle fiber regeneration when they are expressed in adult muscles (16). Differential myosin expression can also be used to distinguish various muscle fiber types as fast type IIA (*Myh2*), fast type IIB (*Myh4*) or slow type (*Myh7*). Slow muscle fibers express higher levels of utrophin and have an increased mitochondrial respiration, both of which have been proposed as mitigating factors in DMD (17,18). Therefore, we tested the hypothesis that the severe pathology seen in the D2-*mdx* mice could be explained by a lack of either regenerating or slow-type muscle fibers.

Myosin expression was quantified at the RNA level in all four mouse strains at the 8-week time point (Fig. 11H). As expected, the two healthy background strains showed low levels of expression of *Myh3* and *Myh8* (markers for regeneration) when compared with the *mdx*-mutant strains. The significantly elevated ($P < 0.001$) levels of *Myh3* and *Myh8* seen in B10-*mdx* mice are consistent with prior reports (19), and the D2-*mdx* strain had similarly high levels of *Myh3* and *Myh8* expression. Both the healthy DBA/2 and mutant D2-*mdx* strains were observed to have significantly higher ($P < 0.01$) basal levels of *Myh7* expression than did the control B10 and mutant B10-*mdx* strains. There were no differences in *Myh4* and *Myh2* expression for either strain.

Myofiber branching and myonuclear domain

Muscle fibers were isolated from the EDL of D2 and D2-*mdx* male mice at 12 weeks of age in order to compare fiber size, extent of

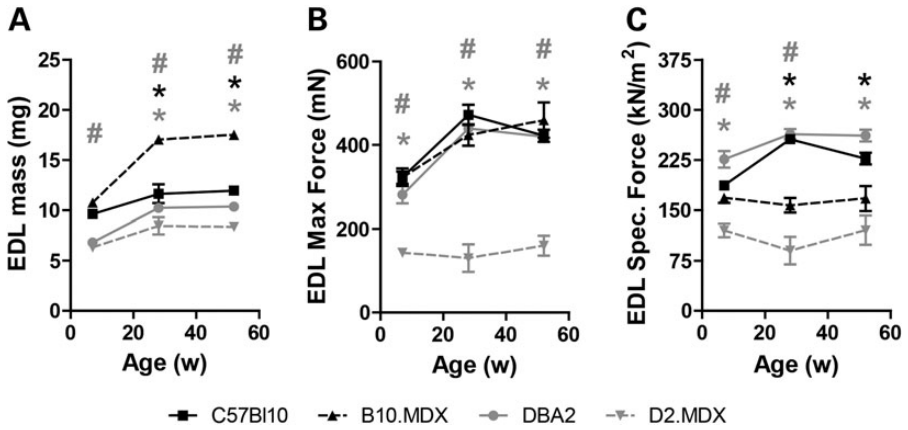

Figure 6. D2-*mdx* mice experience significant muscle weakness at all ages. Force contraction analysis was performed on the freshly dissected EDL muscle of all strains at 7, 28 and 52 weeks at CNMC. Data for the mass of the EDL muscle (**A**), maximum force generation (**B**) and specific force generation (**C**) are shown. The B10-*mdx* mice showed the expected deficit in specific force generation starting at 28 weeks. However, D2-*mdx* mice displayed significant muscle weakness both in terms of maximum and specific force generation beginning at the earliest time point. The mass EDL of the D2-*mdx* mouse was also significantly lower than its wild-type control.

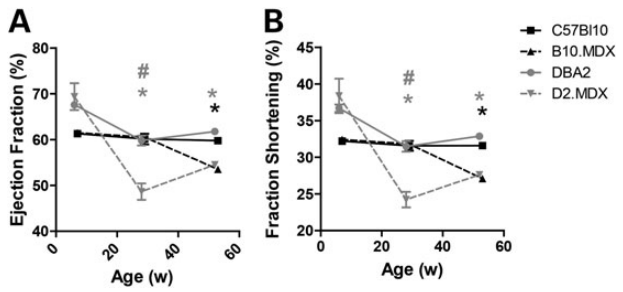

Figure 7. D2-*mdx* mice develop signs of cardiomyopathy earlier than B10-*mdx* mice. Echocardiography was performed by CNMC at 7, 28 and 52 weeks (**A, B**) for each mouse strain. The data analysis showed that the D2-*mdx* mice showed detectable deficits in the EF (A) and shortening fraction (B) starting at 28 weeks, prior to the appearance of any cardiomyopathy in B10-*mdx* mice. The functional deficits in cardiac function were corroborated by histological results as shown in Figure 8B.

branching and myonuclear domain. We calculated fiber size by staining with phalloidin in order to quantify the amount of F-actin per fiber in relation to the number of myonuclei (20). D2-*mdx* were found to have slightly more nuclei per fiber and decreased F-actin content indicative of a smaller fiber size—i.e. D2-*mdx* fibers are atrophic compared with D2 (Fig. 12 C, D, E). Also, D2-*mdx* fibers showed a high incidence of primary and complex branching, which was not observed in the D2 control fibers (Fig. 12A, B). D2-*mdx* fibers contained an average of 290.5 ± 64.4 myonuclei, whereas D2 control fibers contained 262.3 ± 38.6 ($P < 0.001$) (Fig. 12D). Calculation of the normalized ratio of F-actin protein content per myonucleus in each fiber revealed this variable to be significantly lower in D2-*mdx*, than in D2-WT fibers (Fig. 12E); D2-*mdx* had a normalized ratio of 1.659 ± 0.766 whereas the ratio for D2 fibers was 2.299 ± 0.473 ($P < 0.001$), indicating a 28% smaller myonuclear domain in D2-*mdx* than in D2 myofibers.

Discussion

It is well known that the phenotype of a given single-gene mutation in mice is modulated by the genetic background of the inbred mouse strain in which the mutation is maintained. This effect is attributable to modifier genes, which function in combination with the causative gene. Developing congenic mouse strains not only helps us to investigate the effect of genetic background on phenotype but would also facilitate the development of mouse models that more accurately mimic certain features of human disease (21). The commonly used *mdx* mouse models for DMD are on the C57BL/10ScSn background. In these mice, the disease progression in skeletal muscle (with the exception of the diaphragm) is mild when compared with the disease progression in humans. It has previously been shown that transfer of the γ-sarcoglycan-null allele and the *mdx* mutation onto the DBA/2J background confers a more severe muscular dystrophy phenotype (9,10). Therefore, we decided to generate congenic mice carrying the *mdx* 23 mutation on the DBA2/J background. In this paper, we report that *mdx* mice on the DBA2/J genetic background have more skeletal muscle damage and inflammation, as well as an earlier onset of cardiac disease when compared with *mdx* mice on the C57BL/10ScSn background.

Systematic phenotyping of these mice in two different laboratories has revealed consistent and reproducible data. We measured body weights at three ages and tissue weights at the end of the study and found that the body weights did not differ significantly between the two strains of wild-type mice, but the two *mdx* mouse strains showed opposite phenotypes in terms of body weight. The B10-*mdx* mice were generally heavier than the B10 controls, suggesting that some degree of hypertrophy had occurred in the mutant strain. BL10 and B10-*mdx* muscles generally attained maximum size by 12 to 14 weeks, at which point the B10-*mdx* muscle fibers were up to 50% larger than those of the B10 mice (22). Conversely, the D2-*mdx* mice were much smaller than those of the control DBA2 strain, suggesting an atrophic phenotype. Our observations are consistent with a previous report that has shown a significant difference in muscle weight to body weight ratio between D2-*mdx* and control littermates (10). Our study also demonstrates that the decrease in body weight is associated with significant decreases in the weights of the gastrocnemius, TA and quadriceps muscles. The differences in muscle mass were also observed in the sarcoglycan-null mice with a DBA/2 background (10), suggesting that genetic background has an influence on body weight and muscle mass. Evaluation of the muscle fiber diameter of TA muscles suggested that a significantly higher number of smaller fibers were present in the D2-*mdx* mice; thus, the differences in muscle mass are apparently also reflected at the level of the muscle fiber diameters. A major caveat of the B10-*mdx* model is its overt muscular hypertrophy, caused by a strong regenerative response of the skeletal muscle that masks a slow fibrosis and loss of force. Pseudo-hypertrophy in Duchenne patients is more the consequence of the accumulation of fibrotic tissue and fat, and not of the enlargement of muscle fibers; instead, muscle fibers are reduced in size in patient biopsies (23). The atrophy documented in the D2.mdx mice supports the notion that hypertrophy is absent and that muscles are affected in a way more relevant to the human pathology.

We next evaluated whether any of the muscle injury markers were significantly different in the two *mdx* mouse strains, by quantitating serum CK levels as well as EBD uptake by the skeletal muscle. We found significantly increased serum CK levels in both strains when compared with their respective control strains. The serum CK levels were slightly lower in the D2-*mdx* mice than in the B10-*mdx* mice, the likely consequence of the D2.mdx mice being smaller in weight, and having decreased muscle/body weight ratios compared with the B10.mdx, leading to a relatively smaller muscle mass leaking CK enzymes in the serum. CK values in wild-type controls were slightly lower in the Jackson Laboratory measurements, which could be attributed to the use of different methods to dose the enzymatic activity, or more significantly, to differences in the time of day when blood was collected. On the other hand, EBD dye uptake was significantly higher in the D2-*mdx* mice than in the B10-*mdx* mice, suggesting that an increased number of leaky necrotic muscle fibers were present in both mutant strains, particularly in the case of the D2-*mdx* mice. These data seem to contradict previous findings that have shown fewer total necrotic fibers in D2-*mdx* mice (10). However, while we documented EBD uptake in 8-week-old mice, the previous report studied 8-month-old mice. It is expected that, as they age, D2.mdx mice, whose pathology is more severe at an earlier onset, will lose muscle fibers to fibrosis and calcification earlier than B10.mdx mice; in consequence, EBD uptake should be higher in young mice (8 weeks of age) but decreased in older ones (8 months).

To evaluate the effect of genetic background on muscle function, we performed grip-strength measurements and also measured the *in vitro* force contractions of the EDL muscle. We found that forelimb grip strength was significantly reduced in both *mdx* mouse strains at 28 weeks of age. A previous study by

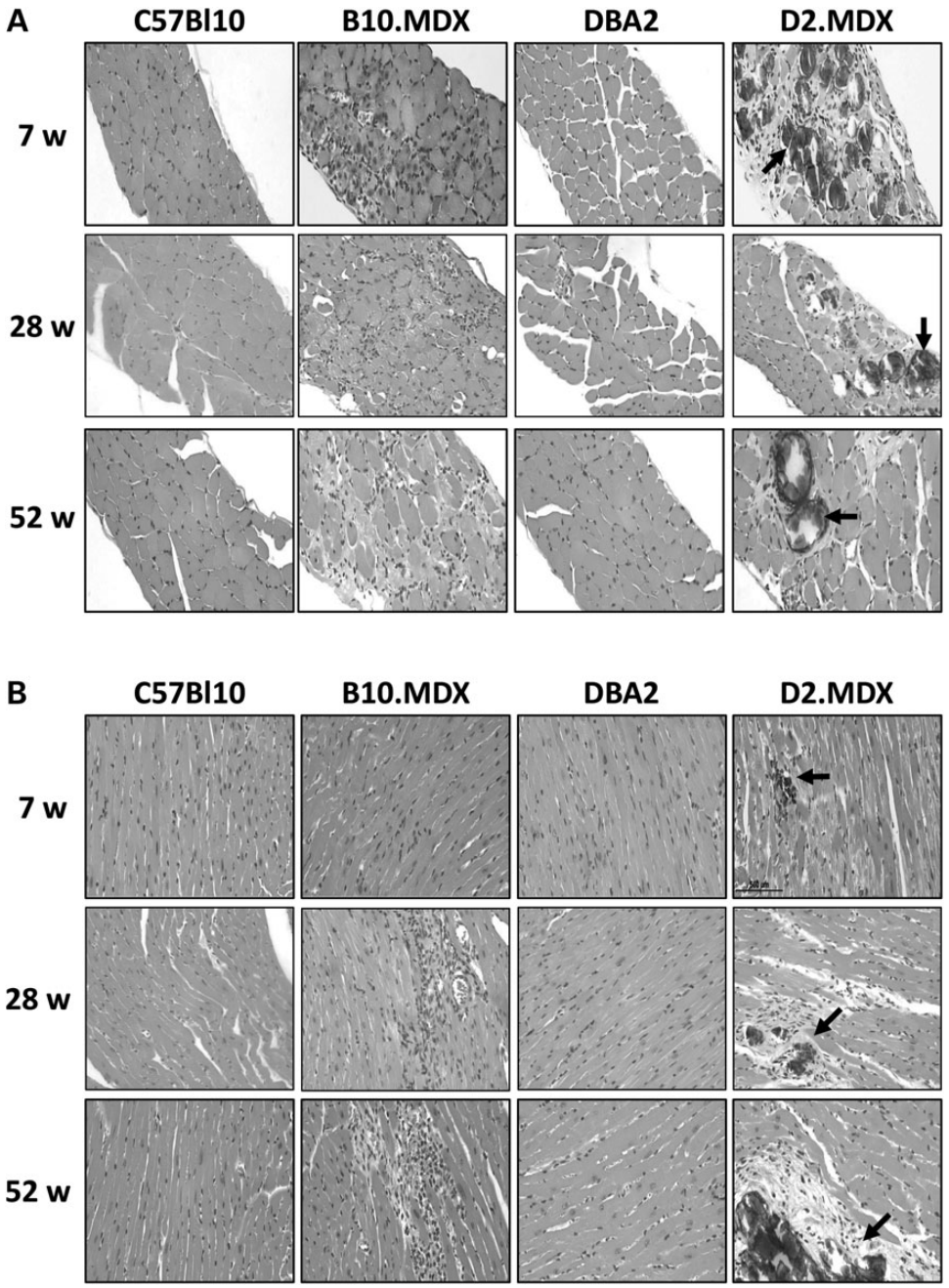

Figure 8. (**A**) Both *mdx* strains show inflammation in the diaphragm at all ages. The diaphragm from each mouse was dissected at 7, 28 and 52 weeks and preserved in 4% formalin prior to H&E staining. Tissue histology was normal for the control C57Bl10 and DBA2 strains. The B10-*mdx* strain showed expected inflammation in the diaphragm. The D2-*mdx* strain displayed inflammation and calcifications (see indicated examples) in the diaphragm at 7 weeks of age. Calcium deposits were only observed in the diaphragm of D2-*mdx* mice. (**B**) D2-*mdx* mice show signs of cardiomyopathy at 7 weeks of age. The heart from each mouse was dissected at 7, 28 and 52 weeks and preserved in 4% formalin prior to H&E staining. Tissue histology was normal for the control C57Bl10 and DBA2 strains. All images show transverse sections of the left ventricle wall. The B10-*mdx* did not show signs of cardiomyopathy until 28 weeks. The D2-*mdx* strain displayed inflammation and calcifications (see indicated examples) in the heart starting at 7 weeks of age. Calcium deposits were only observed in the D2-*mdx* mice.

Fukada *et al.*, 2010 reported differences in grip strength between D2-*mdx* and their congenic controls, but not between B10-*mdx* and B10 control mice (10). It is pertinent to note that our grip-strength assessments were done in two independent groups of mice by two different laboratories. As grip strength is subjected to an animal's volition, we also performed *in vitro* force measures on isolated EDL muscles. The EDL muscle mass of D2-*mdx* mice was, on average, much smaller than that of the B10-*mdx* mice; the maximal force generated by the B10-*mdx* mice was equal to that of both wild-type strains. Thus, the maximal force data obtained for both the BL10 and B10-*mdx* mice were consistent with previous data reported in the literature (24). In contrast, the specific force in both *mdx* strains was much lower than that of the respective control strains; however, the D2-*mdx* mice generated a significantly lower force than did the B10-*mdx* mice, suggesting that the muscle damage is more severe in the D2-*mdx*

mice. Interestingly, the specific force deficit stayed relatively constant and did not change with age in either *mdx* mouse strain. This force deficit was consistent with our histological findings of a more pronounced muscle pathology in D2-*mdx* than in B10-*mdx* mice.

As muscle inflammation is a major component of the disease pathogenesis in dystrophin deficiency, we previously developed a method for detecting inflammation in live animals by using optical imaging of cathepsin B (CTSB) activity. This sensitive method for monitoring inflammation uses a caged near-infrared CTSB substrate, ProSense 680 (15). Using this method, we have now demonstrated that the CTSB activity is higher in both *mdx* strains at 7 weeks of age and decreases significantly by 52 weeks of age, suggesting that inflammation plays an important role early in the disease process in both of these mouse models. This trend in cathepsin activity is likely related to the infiltration of macrophages (a major source of cathepsin release) (25). Indeed, we measured a very strong increase in mRNA markers of macrophages (*Lgals3* and *Mpeg1*) in the muscle of the *mdx* mice, and this increase was more pronounced in the D2 background. These data are also consistent with our previous study in which we found stage-specific remodeling of human dystrophin-deficient muscle, with inflammatory pathways predominating in the early stages and acute activation of TGF-β and failure of metabolic pathways, later in the disease (26). We also found that the early increase and gradual drop in inflammation is reflected in the pro-inflammatory cytokine expression in skeletal muscle (27). Cytokines are differentially expressed in the wild-type strains (both backgrounds). Furthermore, it is known that the DBA/2 strain has an in-frame deletion within the LTBP4 gene that confers a severe disease phenotype, and it has been proposed that its pathogenic effects are mediated by excessive TGF-β signaling. Intriguingly, a polymorphism in LTBP4 has also been implicated in the pathogenesis of DMD (11).

The self-renewal efficiency of satellite cells after muscle injury in the DBA/2 mouse strain has been shown to be lower than that of C57BL/6 mice (10). Therefore, we counted the percentage of centrally nucleated fibers (%CNF) and measured BrdU uptake, and myosin heavy chain subtypes in muscle of our four mouse strains. We found, as expected, that the %CNF and of BrdU-positive central nuclei were significantly lower in the D2-*mdx* than in the B10-*mdx* and, intriguingly, that the total frequency of myonuclei labeled with BrdU was similar between the two strains. The difference is made up by a higher proportion of BrdU-labeled myonuclei located peripherally in myofibers of D2-*mdx* mice. Our protocol is designed to identify myonuclei formed from myogenic cells that had incorporated BrdU in S-phase during the 3-day period beginning 1 week before autopsy. Because we cannot immunostain for Pax7 in the context of the acid treatment entailed by the BrdU staining protocol, we cannot formally rule out the possibility that the peripherally located BrdU-positive nuclei included satellite cells, but, if so, they would be far more numerous than normal satellite cell populations. However, we can still use these data as an index of myogenic activity over this period and conclude that the intensity

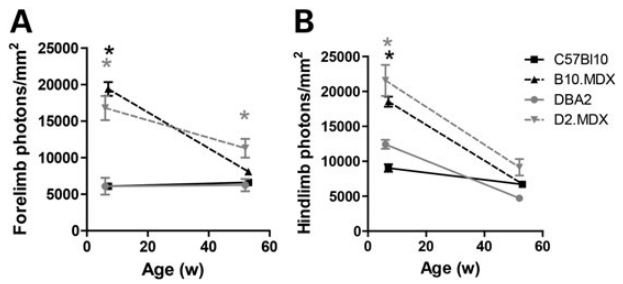

Figure 9. *In vivo* optical imaging confirms increased cathepsin activity and inflammation in *mdx* strains. The cathepsin-mediated cleavage of the ProSense 680 dye serves as a quantifiable marker for inflammation *in vivo*. Sedated mice were imaged at 7 weeks and 52 weeks of age at CNMC. Cathepsin activity was measured in the fore limbs (**A**) and in the hind limbs (**B**). Cathepsin activity was significantly higher in both *mdx* strains at 7 weeks of age when compared with their respective healthy control strains.

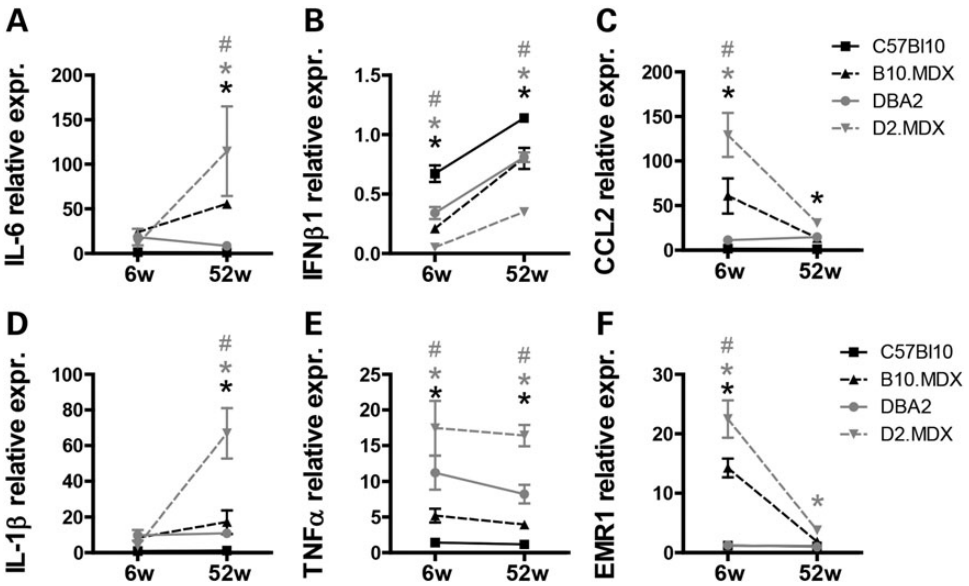

Figure 10. D2-*mdx* mice display significant differences in inflammatory gene expression. We isolated mRNA from frozen TA muscle tissue from 6-week and 52-week-old animals to examine inflammatory gene expression via QRT–PCR. A selection of significantly altered genes is shown in **A–F**. C57Bl10 mice at 52 weeks were used as a baseline for all calculations of changes in relative gene expression. Both D2-*mdx* and B10-*mdx* mice showed the same trends in the expression over time for both soluble cytokines (A–E) and macrophage surface markers (F). Note that the changes in expression in D2-*mdx* mice are greater in magnitude than those in the B10-*mdx* mice.

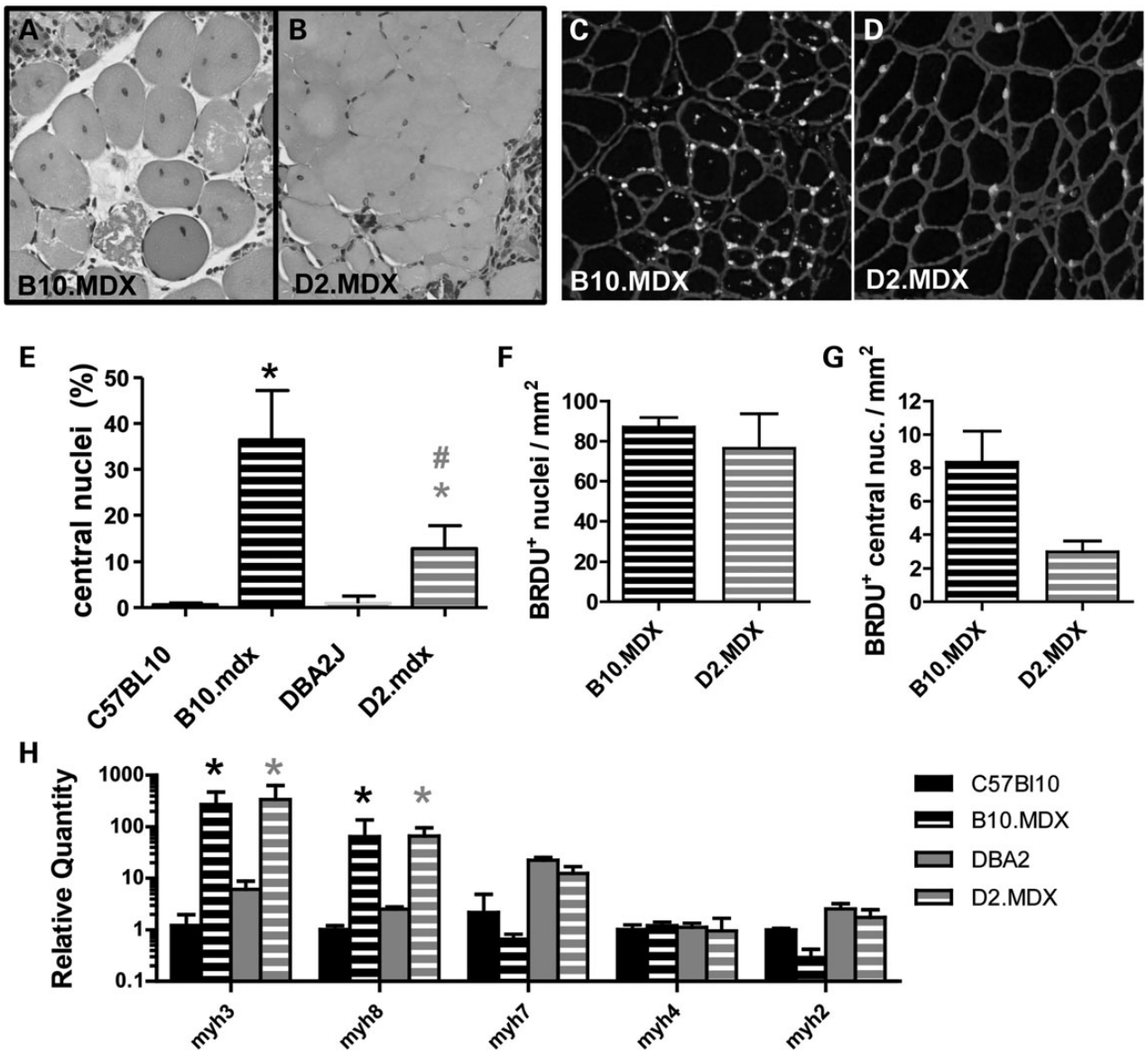

Figure 11. D2-*mdx* mice show a deficiency of central nuclei despite nuclear proliferation in damaged tissues and similar expression of embryonic and neonatal myosin heavy chain subunits, markers of regeneration. Central nuclei are used as markers for successful muscle fiber regeneration. The TA of BrdU-treated animals and prepared for either H&E staining (**A, B**) or immunofluorescence (**C, D**). Frozen sections were stained with anti-BrdU (white colored) and anti-laminin (light gray colored). The proportion of centrally nucleated fibers versus healthy uninjured fibers was quantified for all four strains (**E**). Both *mdx*-mutant strains possessed significantly more central nucleated fibers than their respective controls. The quantification of BrdU-labeled nuclei showed that both strains had similar numbers of newly proliferated cells (**F**) but that the D2-*mdx* mice possessed fewer BrdU-positive central nuclei than B10-*mdx* mice. Myosin gene expression in the TA was determined for all four strains by QRT–PCR (**H**). The D2-*mdx* mice suffered from greater muscle fiber damage than B10-*mdx* mice as measured by EBD uptake. However, levels of embryonic myosin (myh3) or perinatal myosin (myh8) were comparable between the two *mdx* strains. E: $n = 4$ (B10.mdx and D2.mdx), 6 (B10) and 8 (D2) mice per group, average ± SEM, H: $n = 3$ mice per group, average ± SEM.

of regeneration is similar in the two *mdx* strains but that myoblast fusion differs in some way between the two. Counts on isolated myofibers of 3-month-old mice showed similar numbers of myonuclei per fiber in D2 mice to those previously reported in B10 mice (22). However, whereas B10-*mdx* mice contained more than twice as many myonuclei as the B10, the D2-*mdx* myofibers contained only slightly elevated numbers of nuclei (22). In both *mdx* strains, however, the nuclear/sarcoplasmic ratio was markedly lower than in the wild-type strains, suggesting that this may be a common feature of the *mdx* phenotype. These differences were not reflected at the level of the embryonic (*Myh3*) and neonatal (*Myh8*) myosin transcripts expression, which are markers of regeneration. We also tested the hypothesis that D2.mdx has a more severe phenotype because of a lower percentage in slow fibers (that are more resistant to the disease); this was refuted by the experiments and our conclusion is that the origin of the more severe phenotype is to be sought elsewhere.

Unlike the B10-*mdx* mice, we found that the D2-*mdx* mice showed exacerbated calcification in their skeletal muscle, diaphragm and heart tissue; this may be strain-specific, because dystrophic cardiac calcifications are often found in DBA/2 mice, reportedly in association with low plasma magnesium levels

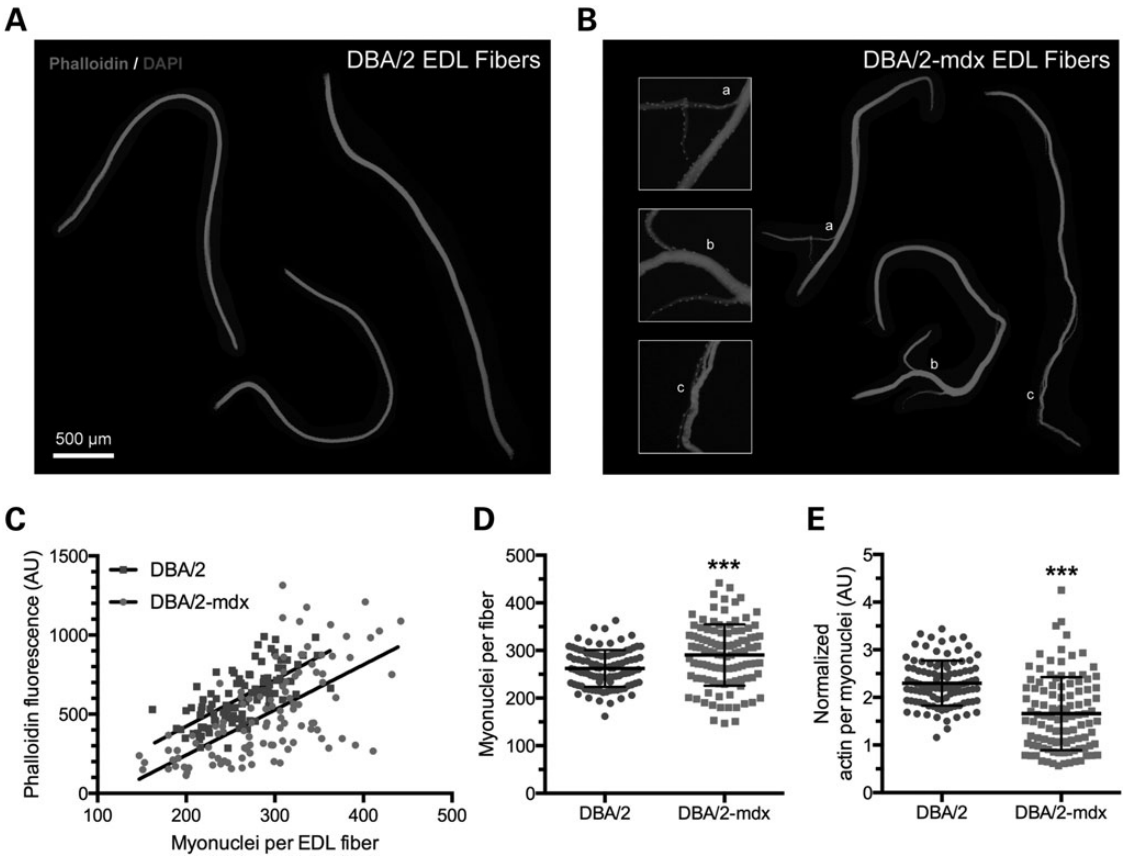

Figure 12. D2-*mdx* mice show increased myofiber branching and decrease in myonuclear domain. EDL myofiber isolation and phalloidin staining for DBA/2 and DBA/2-*mdx* mice at 12 weeks ± 1 week of age (**A, B**). Both primary and complex fiber branch points were observed with high frequency in D2-mdx mice but not D2 (A,B). Total phalloidin fluorescence per myofiber, as an indicator of myofiber volume, plotted against the number of myonuclei per myofiber, displayed as individual data points for both D2 ($n = 3$ mice; total of 102 fibers) and D2-mdx ($n = 3$ mice; total of 108 fibers). (**C**). Myonuclei per myofiber quantified for D2 and D2-*mdx* showing significant increase in average number of nuclei per fiber. Plots show the mean with S.D. (*T*-test, ***$P < 0.001$) (**D**). Normalized F-actin per myonuclei quantified showing a decrease in myonuclear domain for D2-*mdx* compared with controls. Plots show the mean with S.D. (*T*-test, ***$P < 0.001$) (**E**).

(28). Fibrosis, an important feature of muscular dystrophy, has not been measured in this study, but ongoing experiments will address whether fibrosis is more important in D2-*mdx* than in B10-*mdx*—as can be hypothesized based on the increased signaling of the profibrotic TGF-beta pathway previously documented in the D2 background.

We have previously shown that heart dysfunction in B10-*mdx* mice is prominent at 9–10 months of age and is associated with a significantly increased LV internal diameter (at the end of the systole) and a decreased posterior wall thickness. This cardiomyopathy is associated with a 30% decrease in the shortening fraction (29). Our current evaluations of cardiac function now reveal that the D2-*mdx* mice show early cardiomyopathy by 28 weeks of age, considerably earlier than their B10-*mdx* counterparts. These echocardiography results were also consistent with our histological findings. Specifically, we observed cardiac tissue inflammation and damage in D2-*mdx* mice as early as 7 weeks of age, and this damage became progressively worse over time. In contrast, the B10-*mdx* mice did not show any histological signs of cardiomyopathy until 28 weeks, and functional deficits on echocardiography were not seen until the testing at the 52-week time point.

Further exploration of the genetic and physiological differences between the two inbred strains of mice, C57BL10/J and DBA/2J, which account for the differences in the phenotypes of the same mdx mutation, is underway. The first genetic modifier in the DBA/2J genome that has been identified, a partial loss-of-function mutation in Ltbp4, has already been related to an increased atrophy of the dystrophic muscles in this strain: mutant Ltbp4 fails to sequester TGF-β, resulting in an increased signaling by this cytokine that is known to be pro-atrophic on muscle fibers. Moreover, TGF-β is also a known inhibitor of the myogenic differentiation, i.e. of the fusion of myoblasts into myotubes (30). The decreased regeneration potential of the D2.mdx muscles could therefore be explained in part by the increased TGF-β signaling. Whether other genetic determinants explain the difference in myoblasts and/or satellite cells proliferation between C57BL/10 and DBA/2 remains to be elucidated. Differential expression of inflammatory genes has also been documented between DBA/2 and C57BL/6 (31) and could account for the more severe inflammation observed in D2.mdx—a potent driver of the dystrophic phenotype. These differences and others likely to be discovered make the D2.mdx model more relevant to human DMD.

In summary, our data suggest that D2-*mdx* mice have a severe progressive muscle disease with early-onset cardiac deficits. The muscle hypertrophy response that is predominant in the B10-*mdx* model and complicates the study of muscle wasting in this strain is notably absent in the D2-*mdx* model. Thus, this mouse model may be a particularly suitable model for evaluating therapeutics for DMD.

Materials and Methods

Animal husbandry

Animals were housed at a density of up to five males or five females per cage under specific pathogen-free conditions in rooms with a 12-h light/12-h dark cycle at a temperature of 18–23°C and 40–60% humidity. At the CNMC, all mice were handled according the local guidelines established by the Institutional Animal Care and Use Committee (IACUC) of the CNMC in Washington, D.C., and all procedures were carried out under the approved animal protocol. At The Jackson Laboratory, all experiments were conducted in accordance with the protocols described by the National Institutes of Health's Guide for the Care and Use of Animals and were approved by The Laboratory's institutional animal care and use committee. The wild-type strains C57BL/10 (JAX Stock #000476 and #000665; B10) and DBA/2 (JAX Stock #000671; D2) served as the genetic background controls for the two mutant strains C57BL/10ScSn-*Dmd*^{mdx} (JAX Stock #001801; B10-*mdx*) and D2.B10-Dmd^{mdx}/J (JAX Stock #013141; D2-*mdx*), respectively. Control mice at CNMC were descended from stock #000476, and the equivalent controls at The Jackson Laboratory were drawn from stock #000665. Only males were used for this project.

The making of the B10.D2 congenic mouse at The Jackson Laboratory was guided by the use of a 132-SNP panel genotyping at each generation to insure that most of the C57BL10 genome was removed from the D2.mdx mouse, an approach superior to the repeated, but blind, crossing to the DBA/2 background performed before. The panel is composed of an average of six markers distributed across each chromosome. At each generation of a backcross to DBA/2J, mice with the lower number of C57BL10-specific SNPs were selected to be crossed further to inbred DBA/2J mice. At the fifth generation, two founder males we used to establish the B10.D2 colony, which were typed homozygous for the DBA/2J alleles at all SNP loci but from rs13483720 (position 16,660,451 on GRCm38) to rs13483915 (position 102,126,616 on GRCm38), SNPs flanking the DMD gene (position 82,948,870–85,206,141), where they were typed hemizygous for the C57BL10 alleles.

Genotyping

The DBA2 mouse strain has been reported to have a mutation in the LTBP4 gene that may affect muscle function and regeneration (9). Genotyping for this reported deletion mutation was carried out by standard PCR, followed by gel electrophoresis. The product size of the wild-type LTBP4 band is 273 bp, whereas the band for the mutant is only 236 bp. The primers used to identify the LTBP4 status are listed in Table 1. Genotyping of the MDX exon 23 SNP was performed via real-time allelic discrimination using custom-made Taqman® fluorescent-bound primers. SNP genotyping reactions were conducted using the Taqman® SNP Genotyping Master Mix according to the manufacturer's recommendations. The primers used to identify the MDX23 SNP are listed in Table 1.

Table 1. Primers used for genotyping

Primer name	Dye conjugate	Sequence
LTBP4 Forward	n/a	ctgggccacagcctgaac
LTBP4 Reverse	n/a	aagcctttccccacagaaat
MDX23 Forward	n/a	tgaggctctgcaaagttctttgaa
MDX23 Reverse	n/a	catctccttcacagtgtcactca
MDX23 Wild type	VIC	aagccattttgttgctct
MDX23 Mutant	FAM	aagccattttattgctct

Functional and behavioral activities

CNMC grip-strength test

Grip strength for both fore- and hindlimbs was assessed using a grip-strength meter consisting of a horizontal forelimb mesh and an angled hind limb mesh (Columbus Instruments, Columbus, OH) according to a previously published protocol (27). The animals were acclimatized on fore- and hindlimb meshes for 3 consecutive days prior to data collection, and then for 90 s before actual data collection began. Force was measured according to the amount of horizontal force that was required to break the mouse's grip from the mesh surface. Five successful hindlimb and forelimb strength measurements were recorded within 2 min. The maximum values of each day over a 5-day period were averaged and normalized to body weight and expressed as KGF/kg unit.

CNMC behavioral activity testing

Voluntary activity in an open field was measured using an open-field Digi-Scan apparatus (Omnitech Electronics, Columbus, OH) as described previously (27). All mice were acclimatized to the scanning chamber 1 week prior to actual data collection. The data were collected every 10 min over a 1-h period each day for 4 consecutive days. The results were calculated as mean ± standard error for all recordings. The recorded quantitative measures of activity were horizontal activity, vertical activity, total distance and rest time.

CNMC Rotarod testing

The latency-to-fall from the Rotarod apparatus was assessed as described previously (27). In brief, mice were trained on the Rotarod (Ugo Basile, Italy) for 2 days before data collection was begun. Each trial consisted of placing the mouse on the rod at 10 rpm for 60 s (stabilizing period), followed by acceleration from 10 rpm to 40 rpm. Each trial was done twice a day for 3 consecutive days, with a minimum 2-h interval between the data collection times. The latency-to-fall was recorded, and average values were calculated from all six scores.

Jackson Laboratory grip-strength measurements

The strength exerted by the forelimbs of an animal in response to a constant horizontal force was measured. The grip-strength meter (Chatillon-Ametek Digital Force Gauge, DFIS 2, Columbus Instruments) was positioned horizontally, with the triangular metal transducer situated 10 cm above a foam platform. Each mouse was raised toward the triangular transducer, and it instinctively grasped for the bar. Care was taken to ensure the mouse was holding the grip transducer properly with, and only with, both front paws. Once an appropriate grip was observed, the animal was pulled horizontally from the bar. Peak force was measured in kilogram for five consecutive trials per mouse. The maximum force was retained for each animal. For the fatigue quantification, force at the fifth trial was expressed as a percentage of the force at the first trial. Forces were normalized to body weight.

Jackson Laboratory behavioral activity measurements

Voluntary activity measurement consisted of recording 30 min of the horizontal and vertical (rearing) activities in an open field (BiObserve, Germany) for each mouse. Mice were all tested in the morning (9–11 am).

Force contractions on isolated skeletal muscle

Force contraction experiments were conducted on the EDL muscle of the right hindlimb of each mouse. The mouse was anesthetized with an intraperitoneal injection containing ketamine (100 mg/kg) and xylazine (10 mg/kg). The muscles were isolated, and 6–0 silk sutures were tied securely to the distal and proximal tendons. Each muscle was then carefully removed from the mouse and placed vertically in a bath containing buffered mammalian Ringer's solution (137 mM NaCl, 24 mM $NaHCO_3$, 11 mm glucose, 5 mM KCl, 2 mm $CaCl_2$, 1 mm $MgSO_4$, 1 mm NaH_2PO_4 and 0.025 mm turbocurarine chloride) maintained at 25°C and bubbled with 95% O_2–5% CO_2 to stabilize the pH at 7.4. The distal tendon of the muscle was tied securely to the lever arm of a servomotor/force transducer (model 305B, Aurora Scientific) and the proximal tendon to a stationary post in the bath. After removal of the muscle, the mouse was euthanized by gassing with CO_2 according to IACUC guidelines. The muscle was stimulated between two stainless steel plate electrodes. The voltage of single 0.2-ms square stimulation pulses was increased until supramaximal stimulation of the muscle was achieved, and the muscle length was then adjusted to the length that resulted in maximal twitch force (i.e., optimal length for force generation). With the muscle held at optimal length, the force developed during trains of stimulation pulses was recorded, and stimulation frequency was increased till the maximal isometric tetanic force was achieved. For the EDL muscle, 300-ms trains of pulses were used, and a stimulus frequency of ~220 Hz was typically needed to achieve the maximum isometric force. The muscle length was measured with calipers, and the optimal fiber length was calculated by multiplying the optimal muscle length by a constant of 0.45, an established fiber length/muscle length ratio for EDL muscle. The muscle mass was determined after removal of the muscle from the bath. The muscle-specific force, a measure of the intrinsic force generation of the muscle, was calculated according the following equation: specific force = maximal isometric force/(muscle mass × (density of muscle tissue × fiber length)$^{-1}$). The muscle tissue density was 1.056 kg/l.

Echocardiography

In order to assess the cardiac function of mice *in vivo*, we performed echocardiography on sedated mice. Mice were first anesthetized with 5% isoflurane mixed with 100% oxygen at 1.0 l/min flow and then maintained under anesthesia with 1.5% isoflurane/oxygen flow. Ophthalmic ointment was placed on the eyes to prevent drying of the cornea while the mouse was anesthetized and tested. After anesthetic induction, the animals were placed on a thermostatically controlled heated platform, where isoflurane anesthesia was maintained by delivery through a close fitting face-mask. A heating lamp was also used to keep the heart rate and body temperature constant at physiological status during echocardiography. During the examination, the animal's heart rate was monitored through the use of an electrocardiograph. The mouse's heart rate and body temperature were monitored continuously during the scanning. Fur was removed from the ventral surface of the mouse torso with clippers and Nair (Church & Dwight, Ewing, NJ). Echocardiography was performed using Vevo770 ultrasound machine (VisualSonics, Toronto, Canada). The 2-D (B-mode), M-mode and Doppler images were acquired from a modified parasternal long axis view, parasternal short axis view, suprasternal notch view and apical three-chamber view. The heart rate (BPM), fractional shortening, EF, stroke volume and cardiac output were obtained for cardiac function assessment using measurements from the modified parasternal short axis view in the M-mode. Qualitative and quantitative measurements were recorded using Veto 770 offline workstation software, and post-imaging analysis was performed using the VevoStrain analytic software.

Optical imaging

Cathepsin enzyme activity is used as a marker for inflammation, and this activity can be detected *in vivo* by detecting the cathepsin-mediated cleavage of certain dye molecules. Mice were prepared for optical imaging by administering an intraperitoneal injection of 1.5 nmol of ProSense 680 (VisEn Medical), prepared in a total volume of 150 µl, 24 h prior to imaging. On the day of the imaging, mice were sedated using 1.5–2% isoflurane and 100% oxygen before being placed inside the eXplore Optix (GE Healthcare) scanning chamber. The floor of the scanning chamber was continuously heated to maintain normal body temperature. Nair (Church & Dwight, Ewing, NJ) was used to remove fur from the limbs prior to scanning. The scan plane was kept consistent between the mice, at a height that was immediately above the hindlimbs. The scanning area was limited to the limbs. For scanning, a 670-nm excitation frequency was used with a 1.0 mm resolution. Emissions were collected using a 700-nm long-pass filter. The acquired photon intensity data were automatically normalized by the Optiview 2.0 software to account for differences in scanning laser power and integration times selected between mice. The measured cathepsin activity was defined as photon intensity (photon counts/mm^2).

MicroCT scan

The tissue density of formalin-fixed tissues was determined by a MicroCT scan. MicroCT analysis was performed on fixed gastrocnemius, quadriceps, heart and diaphragm tissues using a Sky-Scan 1172 MicroCT (Bruker, Belgium). Imaging was performed at a 40-kV source voltage, 250-µA source current, 295-ms exposure time and 0.4° rotation step, with a 0.5-mm aluminum filter. The imaging resolution size was 9 µm. Three-dimensional reconstructions were performed with Skyscan NRecon and Dataviewer software. For analysis, tissues were selected individually for a polygonal region of interest within the whole tissue area. Tissue density data were obtained from 3D analysis of the selected tissues using Skyscan CT-analyzer software.

Serum creatine kinase activity

At CNMC, blood was collected from mice via cardiac puncture immediately following sacrifice. Serum was separated from other blood fractions by centrifugation and stored at –80°C without EDTA or heparin. CK activity in the serum was measured using the Creatine Kinase Reagent Set from Pointe Scientific, Inc. (Canton, MI) according to the manufacturer's protocol. In brief, 25 µl of serum was pipetted into a volume of pre-warmed detection reagent in a 96-well plate and allowed to incubate for 2 min at 37°C. The absorbance of each well on the plate was then read once per min for 5 min. The average change in absorbance was then used to calculate the concentration of CK in U/l, where 1 U was defined as the amount of CK required to catalyze the conversion of one micromole of creatine phosphate in 1 min at 37°C. All measurements were made on a BioRad xMark spectrophotometer at 340 nm at 37°C using a standard clear 96-well plate. At The Jackson Laboratory, blood was collected by retro-orbital sinus puncture into heparinized glass capillaries, immediately after the last test. Serum was isolated by centrifugation for

10 min at 19,000 rpm. Creatine kinase was measured with a Beckman Coulter AU Clinical Chemistry analyzer.

Histology

H&E staining

Freshly dissected tissues were prepared for histology by fixing tissues with 0.4% neutral buffered formalin (Fisher Scientific) sealed in glass scintillation vials (Fisher Scientific). Fixed tissues were then sent to Hisotserv, Inc. (Germantown, MD) to be mounted in paraffin wax, sectioned and stained with hematoxylin and eosin (H&E). Tissue sections stained with H&E were imaged using an Olympus BX51 microscope with attached Olympus DP70 camera module.

Immunofluorescent staining

Immunofluorescent staining for utrophin and neonatal myosin was performed on gastrocnemius, TA and diaphragm cryosections using the antibodies VP-U579 (Vector Laboratories) and ab49457 (Abcam), respectively. An AlexaFluor® 488-goat anti-mouse IgG1 antibody (Life Technologies) was used as a secondary antibody. Confocal (TCS SP5, Leica) images were acquired at 20× magnification, and the number of positive fibers per microscope field was counted. Counts from three fields were averaged for each muscle.

BrdU staining

For bromodeoxyuridine (BrdU) labeling, the BrdU compound was dissolved in the animal's drinking water (0.8 mg/ml) when the animals were 5 weeks of age. BrdU supplemented water was given for 3 days. Labeled animals were sacrificed 4 days after removal of BrdU water. Frozen muscle tissues were mounted in Optimal Cutting Temperature compound (Tissue-Tek) and cut on a microtome to produce 8 mm-thick cross sections. For BrdU antibody staining in muscle tissues, sections were first allowed to air dry for 5 min before being fixed with HCl. The fixation procedure involved washing slides in Tris-buffered saline + 0.1% Tween-20 (TBST), then submerging them in acetone (pre-chilled to −20°C) for 10 min, followed by a second wash in TBST for 5 min. Fixed slides were then incubated in 2N HCl for 1 h at 37°C, followed by neutralization with 0.15 m sodium borate (pH 8.5) for 10 min at room temperature. Next, slides were washed with TBST and then incubated in blocking buffer (2% BSA, 5% normal goat serum, 0.5% Triton X-100 and 0.1% Tween-20 in PBS) for 1 h at room temperature. Antibody buffer was made by diluting the blocking buffer 1:10 with PBS. Blocked slides were washed in PBS, then incubated with primary biotinylated anti-BrdU antibody [(#B35138, Life Technologies) diluted 1:125 in antibody buffer] and primary anti-laminin [(#L9393, Sigma–Aldrich) diluted 1:125 in antibody buffer] overnight at 4°C. Slides were then washed in PBS before incubation with streptavidin-FITC secondary antibody [(#434311, Life Technologies) diluted 1:600 in antibody buffer] and anti-rabbit Alexafluor-594 [(#A11012, Life Technologies) diluted 1:600 in antibody buffer] for 1 h at room temperature. Images were captured using an Olympus BX61 microscope with attached Olympus DP71 camera module. Counting was performed in a blinded fashion using whole cross sections of the TA muscle, with three whole cross sections per group.

Evan blue dye uptake

Evan blue dye (EBD) uptake by the gastrocnemius was quantified as described previously (32) with minor modifications. EBD (Sigma, E2129) was dissolved in PBS at 10 mg/ml. Each animal received an intraperitoneal injection at 5 µl/g body weight; 24 h after the injection, the gastrocnemius muscles were harvested, homogenized and incubated at 55°C in 1 ml formamide for 2 h. The suspension was cleared by centrifugation at 6000*g* for 5 min, and spectrophotometric absorbance was measured at 620 nm on the cleared lysate. Protein concentration was determined by BCA assay (Pierce, catalog # 23225). Results were recorded as absorbance/microgram of tissue.

Myosin heavy chain identification

For the myosin isoform quantification, assays were performed for the following: myosin 3 (embryonic) (PrimerBank ID 153792648c1), myosin 8 (neonatal) (PrimerBank ID 28893527a1), myosin 7 (slow) (PrimerBank ID 118131045c1), myosin 4 (fast IIB) (PrimerBank ID 67189166c1) and myosin 2 (fast IIA) (PrimerBank ID 205830427c1). All assays were performed using the SYBR® Green method (Life Technologies) on a ViiA™ 7 Real Time PCR System (Life Technologies). GAPDH (PrimerBank ID 126012538c1) was used as a reference gene. Utrophin RNA quantification was performed with the Mm01168866_m1 TaqMan Gene Expression Assay (Life Technologies) multiplexed with GAPDH. Fold changes in expression were calculated by using the average ΔΔCt for the gene of interest in the control B10 group as the reference. Statistical analysis consisted of a two-way ANOVA followed by a Tukey's multicomparison test performed on the ΔΔCt values.

Fiber size measurement and nuclear counting

After dissection, the hindlimbs were fixed in 2% paraformaldehyde in PBS overnight at 4°C. The TA was then dissected and paraffin-embedded. Five-micron-thick microtome cross sections were cut at the level of the belly of the muscle and stained for reticulin. The Gordon & Sweet's Staining Protocol for Reticulin (33) labels collagen III fibrils in the extracellular matrix of the skeletal muscle, allowing the delineation of individual muscle fibers and the measurement of their size on muscle cross sections. Slides were deparaffinized and hydrated, oxidized in 1% potassium permanganate, bleached in 1% oxalic acid, sensitized in 2.5% ferric ammonium sulfate, impregnated with freshly prepared working silver solution (10% silver nitrate, sodium hydroxide and ammonium hydroxide), toned in 0.2% gold chloride solution, placed in 5% sodium thiosulfate, dehydrated, cleared and mounted. Slides were scanned at a ×20 magnification on a digital slide scanner (NanoZoomer 2.0HT, Hamamatsu). A region of interest was drawn on the ventral side of the muscle and analyzed with ImageJ, using the Threshold and Analyze Particle functions, to return the number of fibers and their individual cross sectional areas. An average of 400 fibers were measured per muscle. Fiber size repartition was drawn using a 50-pixel binning. The percentage of fibers with centrally located nuclei was counted manually on the same regions of interest. Fiber numbers were averaged and ranked and plotted as a cumulative rank frequency and significance was tested using the Kolmogorov–Smirnov (K–S) two sample test.

Myofiber isolation, phalloidin staining and F-actin/myonuclear quantification

Single myofibers were isolated at 12 weeks ± 1 week from DBA/2 and DBA/2-*mdx* mice as previously described (20). Extensor digitorum longus muscles were dissected immediately after euthanasia and incubated in 0.2% Collagenase Type 1 (Sigma–Aldrich) in DMEM for 1.5 h at 37°C, to digest the connective tissue. Single

myofibers were liberated by gently pipetting with fire-smoothed wide-mouthed Pasteur pipettes in DMEM pre-warmed to 37°C in dishes pre-coated with 5% BSA. Myofibers were then transferred to a 1.5-ml Eppendorf vial containing 1 ml 4.0% paraformaldehyde and fixed for 10 min at room temperature. The paraformaldehyde supernatant was carefully removed, and the myofibers were washed three times with 1 ml of PBS at room temperature. For phalloidin staining, the myofibers were rinsed with TBS-Tween (Tween 0.1% in TBS). Myofibers were then incubated in blocking buffer (0.5% Triton, 0.1% Tween, 2% BSA and 20% goat serum) overnight at 4°C. The fibers were rinsed three times with TBS-Tween and then re-suspended in Alexa Fluor 594-conjugated phalloidin (Thermo Fisher) at a dilution of 1:40 for 20 min at room temperature. After phalloidin staining, the fibers were rinsed three times and left in the rinse solution overnight at 4°C. The contents of the vial were deposited into a Petri dish and transferred gently onto a microscope slide using a stereo microscope and forceps. The fibers were mounted in Prolong Gold Antifade Reagent with DAPI (Thermo Fisher).We then quantified the numbers of myonuclei and the amount of filamentous actin (F-actin) for DBA/2 and DBA/2-*mdx* ($n = 3$ mice). As most fibrous actin within the fiber is associated with the myofibrillar structures, this is an index of the amount of contractile apparatus. Images were acquired on an Olympus BX61 microscope with a Olympus PlanApo 10× objective and the resulting images (typically 3–5 per fiber) were stitched together with Adobe Photoshop photomerge feature. Phalloidin signal intensity was measured using the ImageJ Macro 'PhAct' (http://rsbweb.nih.gov/ij/macros/) as previously described (20); myonuclear counts were also performed using ImageJ.

Inflammatory marker detection

Jackson laboratory RT–QPCR

Total RNAs were extracted from the TA muscle using the Trizol method, and 800 ng of total RNAs were treated with DNAse and reverse-transcribed, with 40 ng of cDNA used per 10-µl quantitative PCR reaction. For the Jackson Laboratory inflammation marker panel, the following assays were selected from the PrimerBank website [(Spandidos *et al.*), http://pga.mgh.harvard.edu/primerbank/]: TNF-alpha (PrimerBank ID 133892368c1), interleukin-6 (PrimerBank ID 13624310c1), Mpeg1 (PrimerBank ID 133506752c1), Lgals3 (PrimerBank ID 225543162c1), CD53 (PrimerBank ID 161484612c1), CD48 (PrimerBank ID 145966847c1), Lyc6c1 (PrimerBank ID 26353880a1), LTB (PrimerBank ID 161760676c1) and CD11b (PrimerBank ID 132626288c1).

For the CNMC inflammation panel, the following assays were selected from the Life Tech Taqman repository: HPRT1 (Taqman Mm01545399_m1), B2M (Taqman Mm00437762_m1), CD247 (Taqman Mm00446171_m1), EMR1 (Taqman Mm00802529_m1), ICAM-1 (Taqman Mm00516023_m1), IFN-β1 (Taqman Mm00439552_s1), IL-12α (Taqman Mm00434165_m1), IL15 (Taqman Mm00434210_m1), IL1β (Taqman Mm00434228_m1), IL6 (Taqman Mm00446190_m1), CCL2 (Taqman Mm00441242_m1), TNFα (Taqman Mm00443258_m1), Ms4a1 (Taqman Mm00545909_m1) and VCAM (Taqman Mm01320970_m1). The fold changes in expression were calculated by using the average ΔΔCt for the gene of interest in the C57BL/10 group as reference. Statistical analysis consisted of a two-way ANOVA followed by a Tukey's multicomparison test performed on the ΔΔCt values.

Statistical analysis

For the following experiments performed at the Jackson Laboratory, mouse handling and testing, tissue collection and analyses were performed by an operator who was blinded as to the genotype of the mouse: morphometry, CK, EBD uptake, central nuclei and grip-strength measurements, and real-time PCR. Where appropriate, statistical significance was calculated using either Student's *t*-test or two-way ANOVA tests for independent samples with *post hoc* Bonferroni comparisons for each possible pair of groups, unless otherwise noted. Calculations were performed using Prism v5 software (GraphPad Software). Any significant differences ($P < 0.05$) between the two control strains are denoted with the hash symbol. Significant differences ($P < 0.05$) between the C57BL/10 and the B10-*mdx* strains are denoted with a black asterisk symbol. Any significant differences ($P < 0.05$) between the DBA/2 and D2-*mdx* strains are denoted with a gray asterisk symbol (symbol colors correspond to the coat colors for the two background strains).

Supplementary Material

Supplementary Material is available at *HMG* online.

Acknowledgements

We thank Debbie McClellan for the excellent editorial help.

Conflict of Interest statement: K.N. is the president of Agada biosciences, a contract research organization involved in preclinical drug testing in neuromuscular disease models.

Funding

K.N. is supported by National Institutes of Health (5U54HD053177; K26OD011171, P50AR060836-01), Muscular Dystrophy Association, and US Department of Defense (W81XWH-05-1-0616, W81XWH-11-1-0782). G.A.C., K.N. and C.L. are supported by US Department of Defense (W81XWH-11-1-0330).

References

1. Hatzipetros, T., Bogdanik, L.P., Tassinari, V.R., Kidd, J.D., Moreno, A.J., Davis, C., Osborne, M., Austin, A., Vieira, F.G. and Lutz, C. (2014) C57BL/6J congenic Prp-TDP43A315T mice develop progressive neurodegeneration in the myenteric plexus of the colon without exhibiting key features of ALS. *Brain Res.*, **1584**, 59–72.
2. Gallagher, M.D., Suh, E., Grossman, M., Elman, L., McCluskey, L., Van Swieten, J.C., Al-Sarraj, S., Neumann, M., Gelpi, E. and Ghetti, B. (2014) TMEM106B is a genetic modifier of frontotemporal lobar degeneration with C9orf72 hexanucleotide repeat expansions. *Acta Neuropathol.*, **127**, 407–418.
3. Heiman-Patterson, T.D., Sher, R.B., Blankenhorn, E.A., Alexander, G., Deitch, J.S., Kunst, C.B., Maragakis, N. and Cox, G. (2011) Effect of genetic background on phenotype variability in transgenic mouse models of amyotrophic lateral sclerosis: a window of opportunity in the search for genetic modifiers. *Amyotroph. Lateral Scler.*, **12**, 79–86.
4. Heydemann, A., Ceco, E., Lim, J.E., Hadhazy, M., Ryder, P., Moran, J.L., Beier, D.R., Palmer, A.A. and McNally, E.M. (2009) Latent TGF-β–binding protein 4 modifies muscular dystrophy in mice. *J. Clin. Invest.*, **119**, 3703.
5. Sicinski, P., Geng, Y., Ryder-Cook, A.S., Barnard, E.A., Darlison, M.G. and Barnard, P.J. (1989) The molecular basis of muscular dystrophy in the mdx mouse: a point mutation. *Science*, **244**, 1578–1580.

6. Ryder-Cook, A., Sicinski, P., Thomas, K., Davies, K., Worton, R., Barnard, E., Darlison, M. and Barnard, P. (1988) Localization of the mdx mutation within the mouse dystrophin gene. *EMBO J.*, **7**, 3017.
7. Chamberlain, J.S., Metzger, J., Reyes, M., Townsend, D. and Faulkner, J.A. (2007) Dystrophin-deficient mdx mice display a reduced life span and are susceptible to spontaneous rhabdomyosarcoma. *FASEB J.*, **21**, 2195–2204.
8. Stedman, H.H., Sweeney, H.L., Shrager, J.B., Maguire, H.C., Panettieri, R.A., Petrof, B., Narusawa, M., Leferovich, J.M., Sladky, J.T. and Kelly, A.M. (1991) The mdx mouse diaphragm reproduces the degenerative changes of Duchenne muscular dystrophy. *Nature*, **352**, 536–539.
9. Heydemann, A., Ceco, E., Lim, J.E., Hadhazy, M., Ryder, P., Moran, J.L., Beier, D.R., Palmer, A.A. and McNally, E.M. (2010) Latent TGF-β–binding protein 4 modifies muscular dystrophy in mice. *J. Clin. Invest.*, **120**, 645.
10. Fukada, S.-i., Morikawa, D., Yamamoto, Y., Yoshida, T., Sumie, N., Yamaguchi, M., Ito, T., Miyagoe-Suzuki, Y., Takeda, S.i. and Tsujikawa, K. (2010) Genetic background affects properties of satellite cells and mdx phenotypes. *Am. J. Pathol.*, **176**, 2414–2424.
11. Flanigan, K.M., Ceco, E., Lamar, K.M., Kaminoh, Y., Dunn, D. M., Mendell, J.R., King, W.M., Pestronk, A., Florence, J.M. and Mathews, K.D. (2013) LTBP4 genotype predicts age of ambulatory loss in Duchenne muscular dystrophy. *Ann Neurol*, **73**, 481–488.
12. van den Bergen, J.C., Hiller, M., Böhringer, S., Vijfhuizen, L., Ginjaar, H.B., Chaouch, A., Bushby, K., Straub, V., Scoto, M. and Cirak, S. (2014) Validation of genetic modifiers for Duchenne muscular dystrophy: a multicentre study assessing SPP1 and LTBP4 variants. *J. Neurol. Neurosurg. Psychiatry*, **86**, 1060–1065.
13. Bello, L., Kesari, A., Gordish-Dressman, H., Cnaan, A., Morgenroth, L.P., Punetha, J., Duong, T., Henricson, E.K., Pegoraro, E. and McDonald, C.M. (2015) Genetic modifiers of ambulation in the cooperative international Neuromuscular research group Duchenne natural history study. *Ann. Neurol.*, **77**, 684–696.
14. Kornegay, J.N., Childers, M.K., Bogan, D.J., Bogan, J.R., Nghiem, P., Wang, J., Fan, Z., Howard, J.F. Jr., Schatzberg, S.J., Dow, J.L. *et al.* (2012) The paradox of muscle hypertrophy in muscular dystrophy. *Phys. Med. Rehabil. Clin. North Am.*, **23**, 149–172. , xii.
15. Baudy, A.R., Sali, A., Jordan, S., Kesari, A., Johnston, H.K., Hoffman, E.P. and Nagaraju, K. (2011) Non-invasive optical imaging of muscle pathology in mdx mice using cathepsin caged near-infrared imaging. *Mol. Imaging Biol.*, **13**, 462–470.
16. Saad, A.D., Obinata, T. and Fischman, D.A. (1987) Immunochemical analysis of protein isoforms in thick myofilaments of regenerating skeletal muscle. *Dev. Biol.*, **119**, 336–349.
17. Selsby, J.T., Morine, K.J., Pendrak, K., Barton, E.R. and Sweeney, H.L. (2012) Rescue of dystrophic skeletal muscle by PGC-1alpha involves a fast to slow fiber type shift in the mdx mouse. *PLoS One*, **7**, e30063.
18. Roma, J., Munell, F., Fargas, A. and Roig, M. (2004) Evolution of pathological changes in the gastrocnemius of the mdx mice correlate with utrophin and β-dystroglycan expression. *Acta Neuropathologica*, **108**, 443–452.
19. Haslett, J.N., Sanoudou, D., Kho, A.T., Bennett, R.R., Greenberg, S.A., Kohane, I.S., Beggs, A.H. and Kunkel, L.M. (2002) Gene expression comparison of biopsies from Duchenne muscular dystrophy (DMD) and normal skeletal muscle. *Proc. Natl Acad. Sci. USA*, **99**, 15000–15005.
20. Duddy, W.J., Cohen, T., Duguez, S. and Partridge, T.A. (2011) The isolated muscle fibre as a model of disuse atrophy: characterization using PhAct, a method to quantify f-actin. *Experim. Cell Res.*, **317**, 1979–1993.
21. Montagutelli, X. (2000) Effect of the genetic background on the phenotype of mouse mutations. *J. Am. Soc. Nephrol.*, **11**, S101–S105.
22. Duddy, W., Duguez, S., Johnston, H., Cohen, T.V., Phadke, A., Gordish-Dressman, H., Nagaraju, K., Gnocchi, V., Low, S. and Partridge, T. (2015) Muscular dystrophy in the mdx mouse is a severe myopathy compounded by hypotrophy, hypertrophy and hyperplasia. *Skeletal Muscle*, **5**, 1–18.
23. Cavalcanti, G.M., Oliveira, A.d.S.B., Assis, T.d.O., Chimelli, L. M.C., Medeiros, P.L.d. and Mota, D.L.d. (2011) Histoquímica y Análisis Morfométrico de las Fibras Musculares de Pacientes con Distrofia Muscular de Duchenne (DMD). *Int. J. Morphol.*, **29**, 934–938.
24. Lynch, G.S., Hinkle, R.T., Chamberlain, J.S., Brooks, S.V. and Faulkner, J.A. (2001) Force and power output of fast and slow skeletal muscles from mdx mice 6–28 months old. *J. Physiol.*, **535**, 591–600.
25. Takeda, A., Jimi, T., Wakayama, Y., Misugi, N., Miyake, S. and Kumagai, T. (1992) Demonstration of cathepsins B, H and L in xenografts of normal and Duchenne-muscular-dystrophy muscles transplanted into nude mice. *Biochem J*, **288**, 643–648.
26. Chen, Y.W., Nagaraju, K., Bakay, M., McIntyre, O., Rawat, R., Shi, R. and Hoffman, E.P. (2005) Early onset of inflammation and later involvement of TGFbeta in Duchenne muscular dystrophy. *Neurology*, **65**, 826–834.
27. Spurney, C.F., Gordish-Dressman, H., Guerron, A.D., Sali, A., Pandey, G.S., Rawat, R., Van Der Meulen, J.H., Cha, H.J., Pistilli, E.E., Partridge, T.A. *et al.* (2009) Preclinical drug trials in the mdx mouse: assessment of reliable and sensitive outcome measures. *Muscle Nerve*, **39**, 591–602.
28. Van den Broek, F. and Beynen, A. (1998) The influence of dietary phosphorus and magnesium concentrations on the calcium content of heart and kidneys of DBA/2 and NMRI mice. *Lab. Animals*, **32**, 483–491.
29. Spurney, C.F., Knoblach, S., Pistilli, E.E., Nagaraju, K., Martin, G.R. and Hoffman, E.P. (2008) Dystrophin-deficient cardiomyopathy in mouse: Expression of Nox4 and Lox are associated with fibrosis and altered functional parameters in the heart. *Neuromuscul. Disord.*, **18**, 371–381.
30. Massagué, J., Cheifetz, S., Endo, T. and Nadal-Ginard, B. (1986) Type beta transforming growth factor is an inhibitor of myogenic differentiation. *Proc. Natl Acad. Sci. USA*, **83**, 8206–8210.
31. Shen, J., Abel, E.L., Riggs, P.K., Repass, J., Hensley, S.C., Schroeder, L.J., Temple, A., Chau, A., McClellan, S.A. and Rho, O. (2012) Proteomic and pathway analyses reveal a network of inflammatory genes associated with differences in skin tumor promotion susceptibility in DBA/2 and C57BL/6 mice. *Carcinogenesis*, **33**, 2208–2219.
32. Heydemann, A., Huber, J.M., Demonbreun, A., Hadhazy, M. and McNally, E.M. (2005) Genetic background influences muscular dystrophy. *Neuromuscul. Disord.*, **15**, 601–609.
33. James, K. (1967) A simple silver method for the demonstration of reticulin fibres. *J. Med. Lab. Technol.*, **24**, 49.